Chemical Engineering Journal 362 (2019) 830–841

Contents lists available at ScienceDirect

Chemical Engineering Journal

journal homepage: www.elsevier.com/locate/cej

Atmospheric pressure glow discharge for CO_2 conversion: Model-based exploration of the optimum reactor configuration

G. Trenchev[a,*], A. Nikiforov[b], W. Wang[a], St. Kolev[c], A. Bogaerts[a]

[a] Research Group PLASMANT, Department of Chemistry, University of Antwerp, Universiteitsplein 1, B-2610 Antwerp, Belgium
[b] University of Gent, St. Pietersnieuwstraat, Department of Applied Physics, 41, 9000 Gent, Belgium
[c] Faculty of Physics, Sofia University, 5 James Bourchier Boulevard, 1164 Sofia, Bulgaria

HIGHLIGHTS

- A novel plasma reactor for CO_2 conversion is investigated.
- The reactor performance is optimized through computer simulations.
- Two new reactor configurations are developed, showing excellent results.
- A plasma model is developed, showing good agreement with the experimental data.
- The modelling results provide a deep insight into the CO_2 plasma properties.

ARTICLE INFO

Keywords:
Plasma
CO_2 conversion
Atmospheric
Glow discharge
Vortex flow
Modeling

ABSTRACT

We investigate the performance of an atmospheric pressure glow discharge (APGD) reactor for CO_2 conversion in three different configurations, through experiments and simulations. The first (basic) configuration utilizes the well-known pin-to-plate design, which offers a limited conversion. The second configuration improves the reactor performance by employing a vortex-flow generator. The third, "confined" configuration is a complete redesign of the reactor, which encloses the discharge in a limited volume, significantly surpassing the conversion rate of the other two designs. The plasma properties are investigated using an advanced plasma model.

1. Introduction

Mitigating greenhouse gas emissions represents an important problem in today's world. While still being the main propellant for the industrial progress, burning fossil fuels gives an ever-increasing rate of CO_2 emission in the atmosphere. Other processes, such as ammonia production, release excessive CO_2 as well [1]. As a result, finding technological solutions for CO_2 reduction became a rapidly growing research topic in many scientific fields.

Among other emerging technologies, such as electrochemical [2] and biochemical conversion [3], plasma technology is also gaining increasing importance [4,5]. Plasma is an ionized gas, and beside neutral molecules, it consists of electrons, various ions, radicals, excited species and photons. It is typically produced by applying electromagnetic power to a gas, either through a high electric potential difference between two electrodes, or by electromagnetic field resonance. The charged species in the plasma are accelerated by the strong electromagnetic fields, producing a very active medium. Due to their low mass, the electrons are capable of achieving high energy, and they can effectively dissociate CO_2 molecules upon impact, by various mechanisms, e.g., vibrational or electronic excitation, or ionization. The new species emerging in this process (i.e., vibrationally or electronically excited molecules, ions, or radicals) can further contribute to the conversion process. The conversion is most energy-efficient at low gas temperature, as this promotes the (most efficient) vibrational-induced dissociation pathway, by limiting vibrational-translational relaxation [4–10]. Hence, while a sufficient electron temperature is needed (1–2 eV), the overall gas temperature should be kept low (certainly below 2000 K), to create a strong thermal non-equilibrium [4–10].

Many different reactor types are being explored for plasma-based CO_2 conversion, but most research has been performed with microwave [10], dielectric barrier discharge (DBD) [11] and gliding arc (GA) reactors, operating in glow-like or arc regime, which can be AC [12,13] or DC [14,15]. The performance of different reactors varies in terms of

* Corresponding author.
E-mail address: georgi.trenchev@uantwerpen.be (G. Trenchev).

https://doi.org/10.1016/j.cej.2019.01.091
Received 10 October 2018; Received in revised form 22 December 2018; Accepted 15 January 2019
Available online 18 January 2019
1385-8947/

energy efficiency and CO_2 conversion. Microwave plasma reactors exhibit high energy efficiency (around 50%, and even up to 80–90%), but typically only at reduced pressure [4,10]. DBD reactors operate at atmospheric pressure, and show good conversion (up to 30%), but only at a very limited energy efficiency (5–10%) [4,11]. GA reactors combine the advantages of atmospheric pressure operation with good energy efficiency, but their conversion is limited by the fraction of gas that passes through the active arc region. Indeed, in a classical GA discharge, the conversion is typically only around 8%, yielding an energy efficiency around 30% [16]. For this reason, a GA discharge in reverse-vortex flow (RVF) configuration was developed [15], increasing the residence time of the gas inside the plasma. However, this setup still allows only a limited fraction of gas to pass through the arc, thus still limiting the actual CO_2 conversion to 8–9%, with an energy efficiency of about 30% [14]. In addition, it operates in a high-current regime (around 0.5 A), with a high temperature cathode hot spot (around 5000 K) [17], which limits the reactor reliability and brings the discharge too close to thermal equilibrium [4,6,18]. Furthermore, the fast-swirling conductive plasma in such a reactor presents a significant challenge for most DC power supplies, as it acts as a reactive load, and it generates strong magnetic fields [17].

The atmospheric pressure glow discharge (APGD) operates in a stable regime, at low current, i.e., in the range of a few to a few tens of mA. Its discharge volume is relatively small, which leads to a high power density (around 5×10^7 W/m^3), which is comparable to a GA [19]. Typically, APGDs utilize a sharp pin (cathode) facing a ground plate (anode), with gas flowing axially with respect to the pin. The cathode pin concentrates the electric field on its tip, which facilitates ionization and discharge start-up, while its temperature is kept below the melting point by the convective cooling from the gas flow. Typically, a thin layer of strong electric field (around 10^6 V/m) forms at the cathode tip [20,21], and initiates the discharge. This makes the discharge breakdown length (or volume) limited by the maximum voltage supplied (i.e. Paschen's law [22]) and by the electrode shape (i.e. a sharper electrode concentrates the electric field). Such configuration – a sufficient initial electric field to facilitate discharge self-ignition, with a low gas temperature – is very promising for efficient CO_2 conversion, as it allows for a high-degree of thermal non-equilibrium plasma. Furthermore, a low gas temperature is favorable for reducing the vibrational-translational relaxation, as mentioned above [4–9].

Several papers studied the fundamental properties of APGDs. In an extensive review [23], diagnostics were carried out for atmospheric pressure glow micro-plasmas. In [24], diagnostics were performed for a pin-to-plate APGD, with N_2 and dry air. It was concluded that in these conditions the plasma is far from thermal equilibrium, with the vibrational temperature (around 5000 K) significantly higher than the gas temperature (around 2000 K). It is important to note that these properties are very dependent on the gas used. Similar results were obtained in [25], where discharge striations were also reported. Finally, APGDs are a typical subject for studying the process of glow-to-arc transition [26,27].

APGDs are also gaining increasing interest for various applications, such as surface modification [28,29] and gas conversion [30–31]. In [30,31], CO_2 reforming of CH_4 was reported to yield a high conversion, up to around 83%, although for a very low energy efficiency (estimated around 3%). In [32], a conversion up to 20% was obtained for pure CO_2 splitting, with a relatively low energy efficiency (below 10%).

To improve the performance of APGDs (and other types of gas discharge plasmas) for CO_2 conversion, more insight in the underlying mechanisms is clearly needed. This can be obtained by experiments, but also through computational modeling. The detailed plasma chemistry, either in pure CO_2 (with emphasis on the role of the vibrational levels) or in mixtures (e.g., with CH_4), is typically described by 0D plasma chemical kinetics models [7,18,33,34]. However, the latter cannot describe the particular features of reactor design. For this purpose, 2D or 3D plasma dynamics models are required. Some advanced models have been developed for 2D DC plasma sources, such as GAs [35]. The computational load, a main obstacle in such models, has been reduced using the quasi-neutral (QN) approach, where the electron density and the sum of all ion densities are assumed to be equal [36]. This approach allows for more elaborate models, either in 3D [19,37], or utilizing a more complex chemistry, which is required for CO_2 [37,38,39]. However, there exist no detailed models yet to describe the particular features of APGDs, and certainly not with the purpose to improve their performance for CO_2 conversion. In the present paper, we developed such a model, to explain the characteristics of the APGD, including its benefits and limitations for CO_2 conversion. In addition, we performed gas fluid dynamics simulations to develop improved APGD designs.

First the general experimental set-up will be explained (Section 2). Besides the basic APGD reactor design, we developed two modified configurations with improved performance, and the geometry of the three different setups will be presented in Section 3. Their performance, in terms of CO_2 conversion and energy efficiency, will be discussed in Section 4. In Section 5 we try to obtain more insight in the plasma behavior of the APGD and how it results in non-equilibrium CO_2 dissociation, based on a comprehensive plasma fluid dynamics model. Finally, the conclusion is given in Section 6. The paper is accompanied by a supporting information file (SI), including additional data and model details.

2. Experimental set-up

The APGD is powered by a high voltage Technix DC power supply, capable of supplying up to 30 kV at 40 mA, regulated to 0.05% accuracy, with a negative output. A 300 kΩ ballast resistor limits the electric current and sustains the discharge in the glow mode. The flow of CO_2 gas is adjusted by a Bronkhorst mass flow controller. The discharge current in our experiments is varied between 20 and 30 mA. The treated gas is measured by a GAS CompactGC gas-chromatograph (GC; Interscience). The gas composition is captured by the thermal conductivity detector (TCD-B channel) of the GC. A Molsieve 5A and Rt-Q-Bond column were used to separate O_2 and CO. A back-flush configuration for the CO_2 gas protects the 5A column from poisoning. Fig. 1 presents the entire experimental setup.

The CO_2 conversion is obtained by the following formula:

$$X_{CO_2}[\%] = \frac{n_{CO_2(in)} - n_{CO_2(out)}}{n_{CO_2(in)}} \times 100\% \quad (1)$$

where $nCO_{2(in)}$ is the CO_2 concentration without plasma, and $nCO_{2(out)}$ is the CO_2 concentration after plasma treatment. Note that we only measured CO_2 and O_2 as products. In principle, there can also be some O_3 production, but it is considered negligible here, due to the high temperature. We always performed three consecutive measurements, to obtain an average value and standard deviation. The specific energy input (SEI), which is an important parameter to determine the energy efficiency, is defined as:

$$SEI\,[kJL^{-1}] = \frac{Plasma\ \ power\,[kW]}{Flow\ \ rate\left[\frac{L}{min}\right]} \times 60\frac{s}{min} \quad (2)$$

where the flow rate is defined as standard litres per minute (L/min) and the power (P) is the product of voltage (U) and current (I), i.e. P = U*I, as measured on the power supply indicators, subtracting the power loss in the ballast resistor. The energy efficiency is then defined as:

$$\eta[\%] = \frac{\Delta H_R\,[kJmol^{-1}] \times X_{CO_2}[\%]}{SEI\,[kJL^{-1}] \times 22.4\ \ L\ \ mol^{-1}} \quad (3)$$

where ΔH_R is the reaction enthalpy for CO_2 splitting at standard conditions (279.8 kJ mol^{-1}).

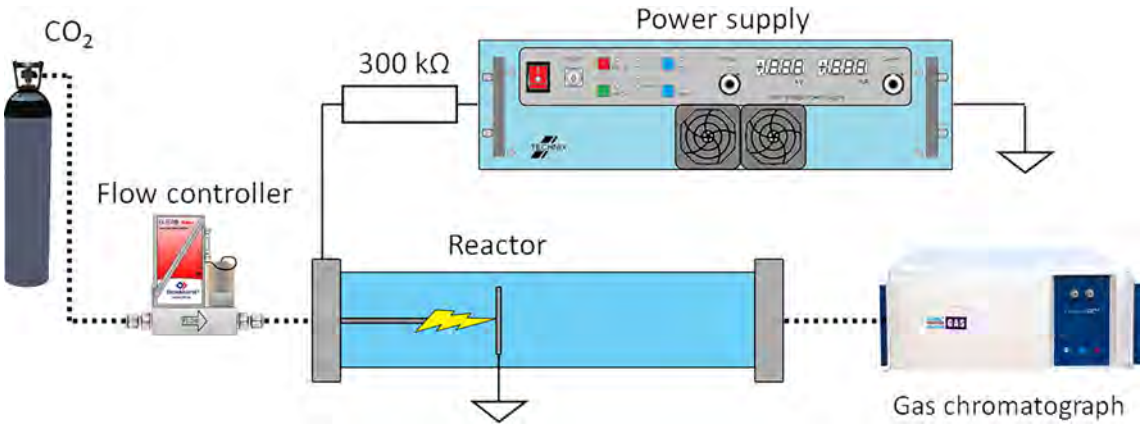

Fig. 1. Experimental set-up. Dotted lines represent gas connections, full lines represent electrical connections. The CO_2 gas is at 99.5 vol% purity, supplied by Air Liquide.

3. Different AGPD reactor configurations: design improvement based on gas fluid dynamics simulations

3.1. Basic APGD

The main body of the APGD reactor consists of an outer quartz tube with total length of 300 mm and internal diameter of 45 mm (see Fig. 2). An internal quartz tube, with a diameter of 10 mm and length of 100 mm contains the cathode pin. The cathode faces an anode plate, which is mounted on three metal pins inside the main tube, but the discharge takes place only in the internal quartz tube. The gas enters the reactor axially, inside the smaller tube, and flows around the cathode pin, which has a diameter of 5 mm and adjustable length of 78 mm. The electrodes are made of stainless steel (Therma 310S), which is heat and corrosion resistant, and with a tungsten tip on the cathode. We performed experiments for an inter-electrode (i.e., pin-to-plate) distance of 18 mm. A larger distance would require a higher applied voltage, but the latter did not allow stable plasma due to the high temperature of the cathode tip (see Section 4).

We should mention that this discharge is specifically called “atmospheric pressure glow discharge” (APGD), but it does not look like a typical low pressure glow discharge in terms of appearance, since it is a constricted discharge and not a diffusive plasma, filling a significant part of the reactor. However, we certainly see distinctive characteristics of a glow discharge, with a high potential drop between the electrodes (several kV), at low current (in the order of mA). For example, an arc discharge would display a low potential drop (few hundred V), and a high current (1A and above) with much higher plasma density. Further reference about this APGD, including some photos of the discharge, albeit in N_2, can be found in Ref. [40].

These experiments turned out that the basic APGD design yields a limited CO_2 conversion (see Section 4), and for this reason, we developed two modified configurations, as will be explained in the next sections.

3.2. Vortex-flow APGD

The vortex-flow APGD makes use of a swirl-flow generating brass ring mounted on the cathode pin (made of stainless steel with tungsten tip, the same as in the basic configuration). The ring has eight holes, oriented in such a direction so that they guide the gas flow to the cathode tip, while also rotating in a vortex (see Fig. 3).

The idea behind it is to (1) slow down the axial gas flow velocity, and increase the residence time of the gas molecules in the plasma, (2) force the gas to the actual discharge zone so that a larger fraction of gas passes the plasma, and (3) lower the gas temperature through increased flow turbulence, as well as cool down the cathode itself, as the brass ring acts as a radiator. The latter will allow to use a larger power input,

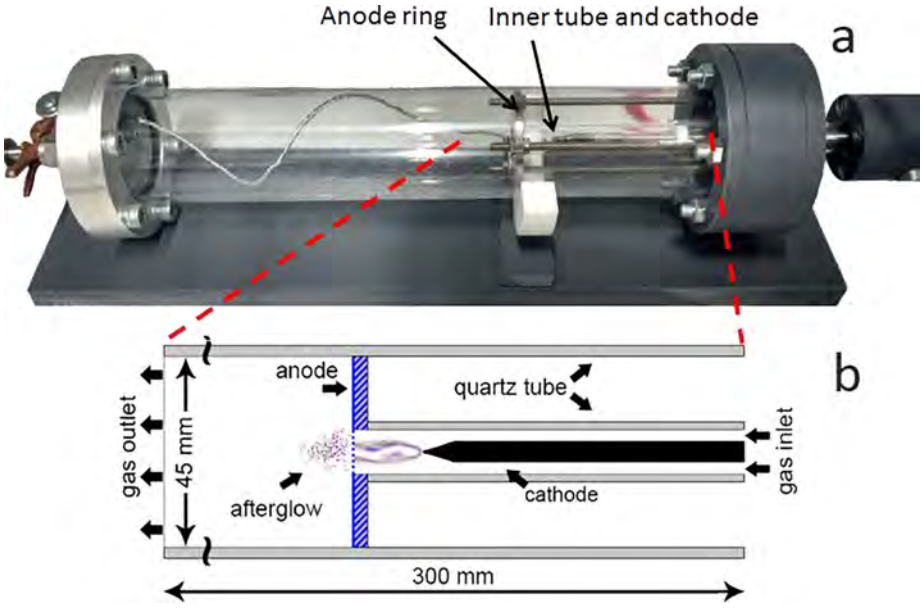

Fig. 2. Photograph (a) and schematic diagram (b) of the APGD reactor. The metal plate holding the anode mesh is mounted on three metal pins. The small internal quartz tube is in the reactor center, where the cathode pin is also visible. The schematic diagram (b) clearly shows the pin-to-plate reactor design, with artistic representation of the discharge and the afterglow.

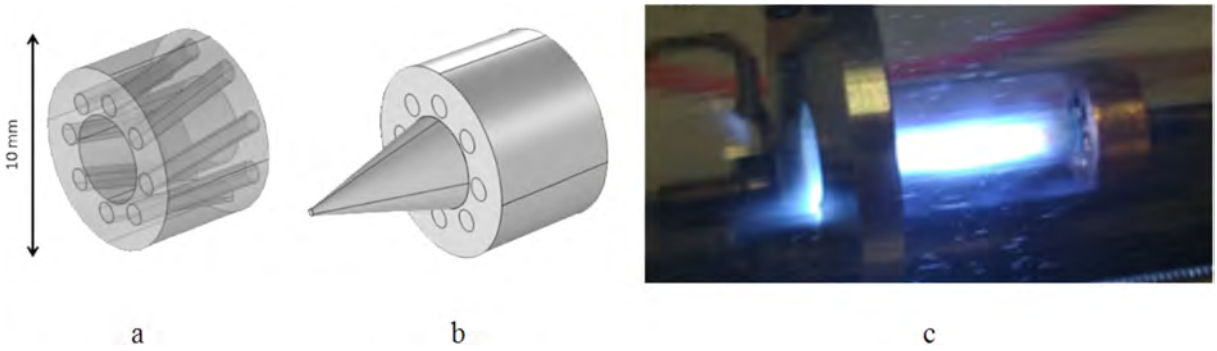

Fig. 3. Vortex generating brass ring, transparent view showing the inclined holes (a), positioned on the cathode tip (b), and in operation (c).

which will lead to a higher conversion (see Section 4), and in addition, a lower gas temperature is beneficial for energy-efficient CO_2 dissociation through the vibrational pathway (see Introduction, [4–10]).

This design was first investigated by gas fluid dynamics simulations, to find out the optimum configuration, such as the inclination angle of the holes. These simulations are based on solving the Navier-Stokes flow equations. More details are given in the supporting information (SI).

As can be seen from Fig. 4(a), without a vortex generator, the gas flow is almost laminar, while a complex rotating flow pattern is observed in the vortex configuration (b). The vortex flow rate through the discharge area was evaluated by integrating the magnitude of the radial and tangential components of the gas flow vector (y and z) over a plane covering the discharge area (a circle with diameter of 2 mm), and the results are shown in Fig. 5, as a function of inclination angle of the holes. The flow rate passing through the discharge area reaches a maximum at 13° inclination angle. Larger inclination angles were not feasible, due to obstruction with the cathode pin. Hence, we selected the 13° inclination angle as the vortex-flow design for production, as we want to reach maximum vortex-flow development. We performed experiments for an inter-electrode distance of 18 mm, as in the case of the basic APGD design, but also for a larger distance of 22 mm, which allows a higher power deposition, and thus higher CO_2 conversion (see Section 4). In contrast to the basic APGD design, the vortex-flow design indeed allowed for a longer inter-electrode distance without melting of the cathode tip, due to the vortex gas flow (see Section 4 below).

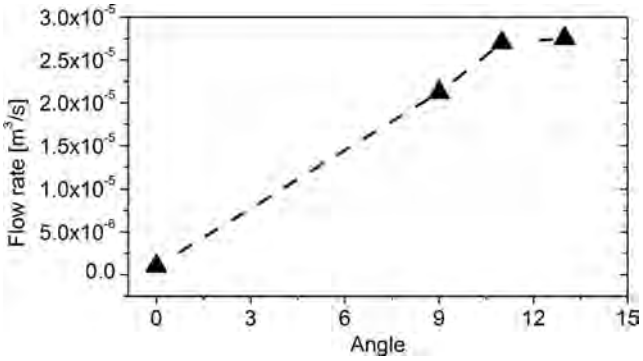

Fig. 5. Dot product (magnitude) of the tangential and radial flow vectors passing through the discharge area, as a function of inclination angle of the eight holes in the vortex-flow APGD configuration.

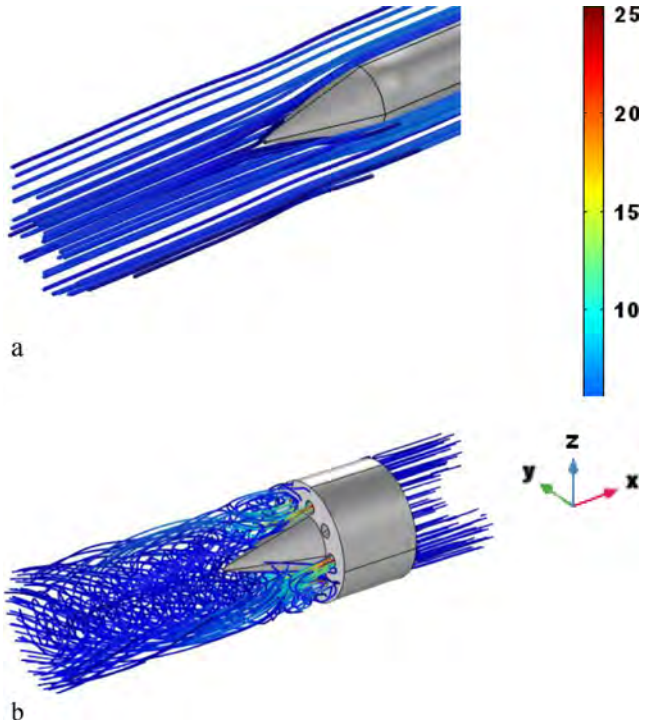

Fig. 4. Design process of the vortex-flow APGD through gas fluid dynamics simulations. The basic configuration (a) with no vortex generator shows typical laminar flow lines. Configuration (b), with an inclination of the vortex-generating tubes of 13°, shows complex rotating flow patterns.

3.3. Confined APGD

The third configuration of the APGD is based on the assumption that still only a limited part of the gas actually flows through the discharge zone. This is clearly the main limitation in GA plasmas, as demonstrated by the fluid dynamics simulations for a gliding arc plasmatron (GAP) [19,37], and it is also observed from the model for the previous two APGD designs in our current work (see further). As a solution, we have encapsulated the entire discharge in a narrow ceramic tube. The tube channel matches the discharge dimensions, as obtained from our plasma model calculation (see Section 5 below), i.e. no gas can pass through without being activated by the plasma.

Fig. 6 illustrates this so-called “confined” configuration of the APGD. The high-temperature ceramic tube with inner radius of 2.5 mm seals tightly with the grooved cathode pin after heat expansion. The entire cathode is made from steel Therma 310S. The gas is delivered to the groove with the same inner quartz tube (with a diameter of 10 mm) as shown in Fig. 2. In this way, the groove acts as a small channel for the gas, conducting flow at high velocity. The distance between the tip of the cathode and the anode plate was again 22 mm, like in the vortex-flow design. With this configuration, two important properties are obtained: a simple, reliable design for confining the discharge, and an effective cooling for the cathode pin, which will allow using higher power input in the plasma. Indeed, even with a steel cathode, 30 mA of current at a flow rate of 1 L/min is possible without melting due the

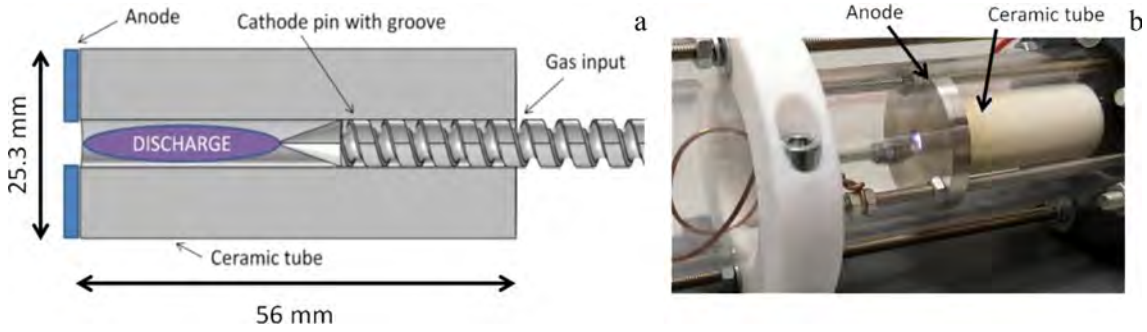

Fig. 6. Schematic diagram of the "confined" APGD, illustrating the internal configuration of the device (a). Photograph of the reactor in operation (b).

active cooling from the high gas flow velocity along the grooves.

Based on the average axial gas flow velocity for all three reactor configurations, we estimate the gas residence time in the discharge zone to be 10 ms, 13 ms and 50 ms for the basic, vortex and confined setups, respectively. The gas temperature is around 2500 K in the discharge centre, and 437 K average in the reactor volume (see further details in the modelling section).

4. Performance of the APGD configurations: CO_2 conversion and energy efficiency

We present here the results for the CO_2 conversion and energy efficiency in the three different configurations, for three different values of electric current. The CO_2 conversion is evaluated by means of gas chromatography.

A vital assessment of the actual discharge regime is its current-voltage characteristic. Fig. 7 presents the measured voltage as a function of the fixed current source for the three different configurations, each within its operation limits. As can be seen from the graph, the voltage drop between the electrodes tends to remain fairly high, but is decreasing steadily with higher current. A glow-to-arc transition would be marked by a sudden voltage peak, followed by a rapid drop. The "confined" APGD was even tested up to 35 mA, with no signs of arcing, which assures that the reactor operates in the glow regime. As it is shown on the graph, the minimum operating current for the 18 mm APGD is 10 mA (11 mA for the confined variant). Below this value, discharge self-pulsing would occur.

Fig. 8(a) shows that the basic APGD yields a conversion around 3.5–4.5%, for an inter-electrode distance of 18 mm. As mentioned in Section 3.1 above, a longer inter-electrode distance would naturally increase the required potential drop over the discharge, and hence the specific energy input (SEI), and thus the CO_2 conversion, as the latter

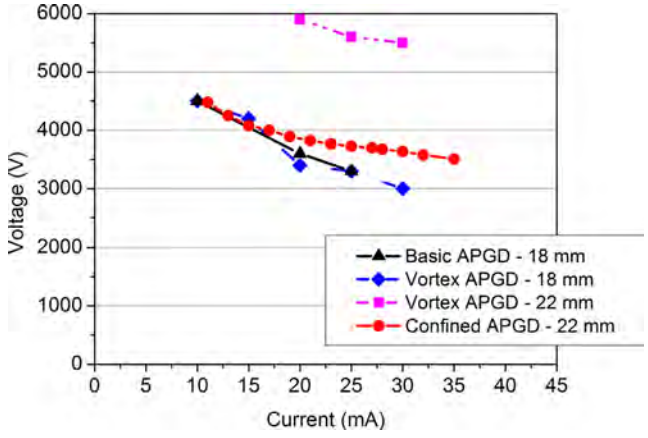

Fig. 7. V-I (voltage vs. current) characteristic of the three APGD variants, indicating also the cathode-anode distance.

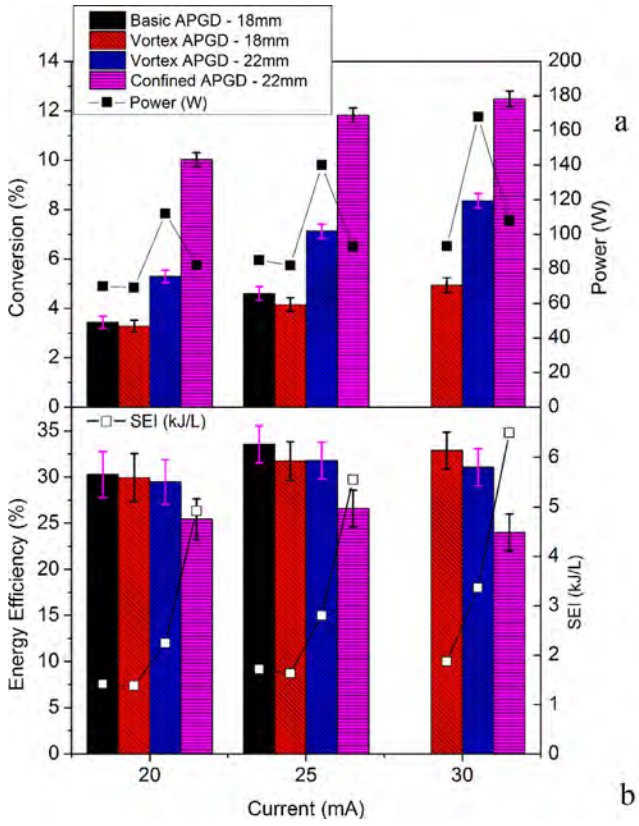

Fig. 8. CO_2 conversion (a) and corresponding energy efficiency (b), for the basic, vortex-flow (with two different inter-electrode distances) and confined APGD, for three different values of discharge current. The flow rate is 3 L/min in the basic and vortex-flow design, while it is 1 L/min in the confined design. The power input and SEI for the different cases are plotted as well, with the corresponding values indicated in the right y-axis of (a) and (b), respectively. The error bars are quantified from the basic accuracy of the instruments, and the number of measurements per data point (3), using standard formulas.

typically rises with SEI (although at the expense of the energy efficiency) [4]. However, the basic APGD is unable to sustain a stable plasma at higher voltage, or current above 25 mA, due to the critically high temperature (at the melting point) of the cathode tip.

This problem is solved with the vortex-flow APGD: as it acts as a radiator to the cathode, it allows for higher power input. This is beneficial for the CO_2 conversion. Fig. 8 indeed illustrates that the vortex-flow APGD can reach higher current and power (30 mA and more than 160 W vs. 90 W for the basic design), and can also be operated at longer inter-electrode distance (22 mm). Thus, it is not surprising that the high SEI of the vortex-flow configuration with 22 mm inter-electrode distance and 30 mA current yields a higher CO_2 conversion, i.e., around 8.3%.

Finally, the confined APGD allows us to reach a CO_2 conversion up to 12.5% at 30 mA. This is a significant improvement compared to both the basic and vortex-flow APGD configurations. At 20 and 25 mA, an enhancement factor of around 3 is obtained compared to the basic design, and around 2 with respect to the vortex-flow design. At 30 mA, an enhancement of a factor 1.5 is obtained with respect to the vortex-flow design, while the basic design was not stable at 30 mA, due to a too high cathode temperature, with the risk of cathode melting. The main reason for this higher conversion is the fact that a larger fraction of gas passes through the active plasma, as the plasma fills up the entire discharge region (see Fig. 6). In addition, the high SEI (6.48 kJ/L at 30 mA, compared to 3.36 kJ/L in the vortex-flow design, for 22 mm inter-electrode distance; see Fig. 8(b); right y-axis) also explains the higher conversion. Indeed, as mentioned above, the specific design of the confined APGD allows for efficient cathode cooling, and thus enables this configuration to operate at high power input (above 100 W) with a low flow rate (1 L/min).

However, this higher conversion comes at the price of a lower energy efficiency, as illustrated in Fig. 7(b). The energy efficiency is nearly 30% for the basic and vortex-flow designs at 20 mA, and even above 30% at 25 and 30 mA, while it drops to 25% at 20 mA, 26.5% at 25 mA and 24% at 30 mA, for the confined APGD. Two main factors contribute to this efficiency loss. First, the plasma is in direct contact with the walls (see Fig. 6), which means that energetic electrons and ions will lose energy and transfer heat upon impact with the ceramic walls. Indeed, we observed that the ceramic piece heats up significantly (over 100 °C), despite being relatively non-conductive to heat. The second reason is that at high SEI, the discharge is closer to thermal equilibrium, which will inherently lower the energy efficiency, as the most energy-efficient vibrational-induced dissociation pathway is not fully explored [4–10]. In general, we can conclude from Fig. 7(a) that the conversion does not rise to the same extent as the SEI, for both the vortex-flow design and especially the confined design, and this explains the slight drop in the energy efficiency (see Fig. 8(b)), because the latter is defined by both the conversion and SEI (see Eq. (3) in Section 2 above). Nevertheless, the drop in energy efficiency compared to the basic and vortex-flow designs is at maximum only around 20%, which is clearly lower than the enhancement factors observed for the conversion, so we may conclude that the confined design overall yields the best results.

In Fig. 9, we compare our results with the best results obtained in various types of plasma reactors from literature. The figure is adopted from [4], with our data points added. It is clear that the APGD does not provide "record values", both in terms of conversion and energy efficiency, but still performs rather well, significantly surpassing DBDs in energy efficiency, and achieving a higher conversion than most GA reactors. Note that the best results presented in Fig. 8 were obtained with microwave (MW) and RF discharges, but these record values were reported in the 1980's and could not yet be reproduced since then. Moreover, they were obtained at reduced pressure, where it is easier to reach thermal non-equilibrium, and thus higher and more energy-efficient CO_2 conversion [4–10]. However, the reduced pressure operation requires vacuum equipment, which is less convenient for industrial exploitation, and it presents an additional cost, not included in the energy efficiency shown in Fig. 9. At present, atmospheric pressure reactors seem to be unable to reach a CO_2 conversion above 20% with reasonable energy efficiency. The APGD, particularly in the "confined" configuration, gets closer to this boundary, with a conversion of 12.5% and corresponding energy efficiency around 25%.

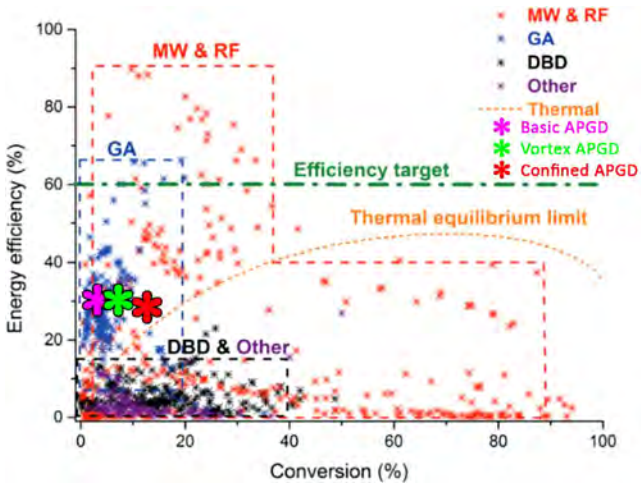

Fig. 9. Comparison of our results, in terms of energy efficiency vs CO_2 conversion, with data collected from literature for CO_2 conversion by different plasma reactors, adopted from [4]. In addition, also the energy efficiency target and thermal equilibrium limit are presented (see text).

As no other atmospheric DC plasma reactor seems to offer such a combination of CO_2 conversion and energy efficiency, we believe that the confined APGD is quite promising for practical applications, also in view of its simple design, although further improvements will be needed to make it competitive with other emerging technologies. Indeed, the energy efficiency is still below the efficiency target, as defined in [4]. Nevertheless, the latter was defined for pure CO_2 conversion, while the results are typically better for the combined conversion of CO_2 and CH_4 (dry reforming of methane, DRM) [4]. In future work, we plan to investigate the performance of our APGD for DRM, and we also plan to develop further improved designs, based on computer modeling. Finally, it is worth to mention that our results are clearly above the thermal equilibrium limit, which is also indicated in Fig. 9. This illustrates that the CO_2 conversion in our APGD is due to non-equilibrium plasma processes, and not just due to thermal conversion, as will be discussed below.

5. Non-equilibrium plasma-induced CO_2 conversion: insights from plasma modelling

In this paper, we presented three different APGD configurations, which demonstrate a difference in conversion performance (see previous section). The basic APGD shows quite low conversion around 4.5%, which is limited by the low power handling ability of the reactor. The vortex-flow APGD allows a larger inter-electrode distance, and thus raising the power input (hence, SEI) by 50%. Therefore, it reaches a conversion up to 8.3%. Finally, the confined APGD reaches a conversion of 12.5%, because it can handle a further increase in SEI, and especially because it allows all gas to pass through the plasma. These configurations were developed based on gas fluid dynamics calculations, as explained in Section 3, but a gas flow analysis alone is insufficient to explaining the behavior of the plasma and the underlying mechanisms for the higher CO_2 conversion. Therefore, we investigate here the nature of the discharge through detailed plasma fluid dynamics modeling.

We developed a fluid dynamics model, very similar to the model presented in [37] for a GAP. It is based on solving the Navier-Stokes equations to obtain the gas flow pattern, while the plasma model is based on the drift-diffusion approximation, and it assumes quasi-neutral plasma [36]. As the CO_2 plasma chemistry is too extensive for a 3D geometry [37], we have to limit ourselves to a 2D model. For this reason, the model can only be applied to the basic design, as the latter is characterized by a laminar flow with a pin-to-plate configuration, which is cylindrically symmetrical (Fig. 2), allowing to use a 2D axi-symmetric approach. Indeed, the vortex motion originating from the two other designs cannot be properly described in 2D, but based on our previous experience [36], we believe that the present model is sufficient to predict the plasma behavior, and to elucidate the underlying mechanisms (and limitations) of the CO_2 conversion. Detailed information on the modelling method, as well as the chemistry included in the

Table 1
CO_2 plasma species included in the model.

Ground state neutrals	CO_2, CO, C, O_2, O
Charged species	e, CO_2^+, O_2^+, CO_3^-, O_2^-, O^-
Excited species	CO_2 (25 vibrational states*, 1 electronic excitation state), O_2 (3 vibrational states)

* Combined in three groups, following the level lumping method of [38,41].

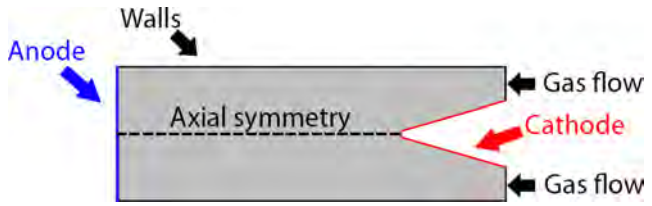

Fig. 10. Schematic illustration of the boundary conditions in the plasma model.

model, is available in the supporting information (SI). The plasma species considered in the model are listed in table 1.

Fig. 10 describes the boundary setup in the plasma model geometry. This is a small excerpt of the entire reactor, covering only the parts with actual plasma. As mentioned above, an axially symmetric approach is used, i.e. with cylindrical coordinate system.

First, to assess the model capabilities, we compare in Fig. 11 the measured and calculated CO_2 conversion and energy efficiency as a function of discharge current for the basic APGD design. The conversion in the model is obtained by integrating the species density over the reactor output, while the energy efficiency is derived from the conversion, power and flow rate, and formulas (2) and (3). Note that the calculation results also contain a data point at 22.5 mA. A higher current (e.g., 30 mA) leads to model instability, consistent with the experiments.

The calculated and measured conversions and energy efficiencies are both in quite good agreement, showing that the model presents a realistic picture of the plasma characteristics affecting the CO_2 conversion (see below). While the calculated conversion is slightly underestimated, the energy efficiency is somewhat overestimated, and this can be explained by the model approximations. Indeed, we use a quasi-neutral model, in which the plasma sheath, i.e. the cathode layer, is not explicitly included. Hence, the voltage drop across the sheath is not accounted for. As a result, the model predicts a lower overall voltage drop across the discharge. Indeed, while the experimental voltage drop is 5.6 kV (at 25 mA, 22 mm), the calculated value (also at 25 mA) is only

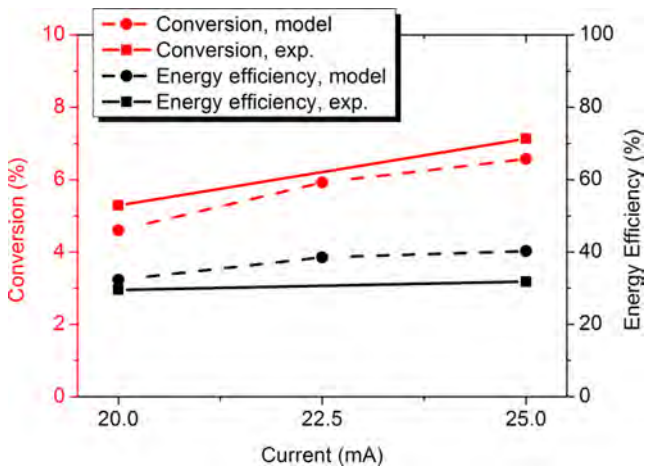

Fig. 11. Comparison of calculated and measured CO_2 conversion and energy efficiency as a function of discharge current, for the basic APGD design.

4.2 kV, as can be deduced from the calculated potential distribution, presented in the SI (Fig. S2). Hence, this is 25% lower than in the experiments. Since the power input is calculated as the product of voltage and current, it is also underestimated by 25%, explaining why the calculated energy efficiency is somewhat higher than the measured values in Fig. 11. However, we want to stress that our model is fully self-consistent across all parameters, with only the current as primary input, and self-consistently calculating the power from the voltage drop, so this comparison gives a thorough assessment of the real predicting capabilities of our model.

As our model yields a reasonable agreement with measured conversion and energy efficiency, we believe it presents a realistic picture of the plasma characteristics affecting the CO_2 conversion. This includes the gas temperature, the electron density and temperature, the vibrational temperature, the electric field, the species densities and the reaction mechanisms responsible for the CO_2 conversion. Thus, we will now present these characteristics, to better understand the underlying mechanisms of CO_2 conversion in the APGD.

Fig. 12 illustrates a gradient-mapped photograph of the basic APGD reactor in operation (a), as well as the temperature profile obtained from the model (b). The close relation between the measured plasma luminosity (a) and the calculated gas temperature (b) is very obvious. The peak gas temperature (at the cathode tip) reaches 2600 K, but the value remains fairly uniform around 2400–2500 K along the discharge axis. In [42], an APGD in air was investigated by means of spectroscopy, measuring a rotational temperature of up to 2000 K. Hence, our calculated value is slightly higher, which can be explained by the differences in reactor design. In addition, it would be better to compare with a CO_2 plasma, but such data are not available. Indeed, measuring the rotational temperature in CO_2 plasma is very difficult without add-in gases (typically N_2), which affects the overall accuracy.

When we compare the calculated gas temperature in this APGD with values obtained in GA plasmas, we can conclude that similar values are reached in a classical GA. For instance, in [43] a gas temperature of 2600 K was measured for a classical GA in air. However, in a gliding arc plasmatron (GAP), a much higher gas temperature (around 3000 K [37]) was calculated for CO_2, and in [17] the measured value in N_2 was reported to be even 5500 K. Hence, the gas temperature in the APGD seems to be significantly lower than in a GAP. This is beneficial for efficient CO_2 conversion, because (i) it might give less vibrational-translation relaxation losses, and (ii) the recombination reaction of $CO + O_2 \rightarrow CO_2 + O$ becomes less important at lower temperatures (with a rate constant of 1.28×10^{-12} $\exp(-12800/T_{gas})$, see table S5 in SI).

Fig. 12(c) illustrates the calculated electron density profile (also called plasma density). Obviously, the maximum electron density (around 2×10^{18} m^{-3}) is at the cathode tip, due to the electric field enhancement in this region (see below). A plasma density in the order of 10^{18} m^{-3} has also been reported for APGDs in literature, i.e., 10^{18} for an APGD in N_2 [40], and around 5×10^{18} m^{-3} for an APGD in helium [44]. It is clear from Fig. 12(c) that the plasma is concentrated near the cathode tip, and hence, the discharge does not fill the entire reactor volume. Thus, a significant amount of gas will pass between the plasma and the walls, being untreated by the plasma, hence confirming our conclusions made in Section 4 above. As already explained in Section 3, this is the reason we developed the confined APGD configuration (Fig. 6 above), which fully encapsulates the discharge in the reactor volume.

Fig. 13(a) shows that the electron temperature in the discharge is about an order of magnitude higher than the gas temperature (i.e. 1.9 eV or 20,000 K vs. 2500 K), which means that the plasma is in thermal non-equilibrium. For comparison, in [25] an electron temperature of 1.4 eV was reported for a low-current (10 mA) APGD in N_2. Hence, the electrons have sufficient energy to activate the CO_2 molecules by electron-impact vibrational excitation, leading to CO_2 splitting. At the cathode tip, the electron temperature reaches 3 eV in a very small region, due to the enhanced electric field at the sharp edge.

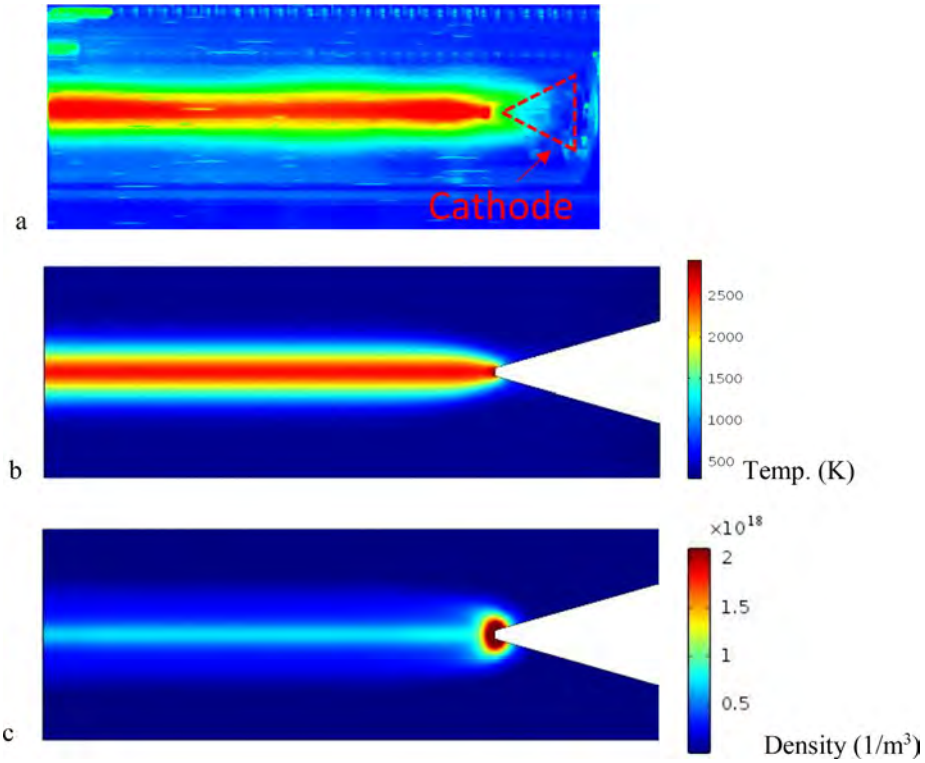

Fig. 12. Gradient-mapped photograph of the basic APGD, illustrating the measured plasma luminosity (in arbitrary units) (a), the calculated gas temperature profile (b), and electron (or plasma) density (c) at 25 mA and 3 L/min.

Although this is a very small, localized region, it could have some impact on the overall CO_2 dissociation through high-energy electron impact electronic excitation. However, the region of high-energy electrons is relatively small (see Fig. 13(a)), which explains why this process plays a minor role in the CO_2 dissociation (see below).

In Fig. 13(b), we plot the calculated electric field profile in the reactor. It is depicted as reduced electric field, i.e., electric field divided by gas number density, expressed in units of Td (1 Td = 10^{-21} V m^2). This is done because the reduced electric field is a very important parameter to characterize the CO_2 conversion ability of gas discharge plasmas [4,9]. Indeed, reduced electric field values below 100 Td (typical for MW and GA plasmas) are known to give rise to electron temperatures (around 1–2 eV) most suitable for vibrational excitation, which is the most energy-efficient CO_2 dissociation pathway, while values above 100–200 Td (characteristic for DBD plasmas) mainly result in electronic excitation-dissociation and ionization, due to the higher electron temperatures produced [4]. It is clear that the APGD gives rise to a reduced electric field around 60 Td in the discharge center, which is thus very beneficial for vibrational excitation due to the produced electron temperature of 1.5–2 eV (see Fig. 13(a)), explaining the good energy efficiency reached in our experiments (see Fig. 8(b) above). A small area around the cathode tip shows a higher value, above 100 Td, which produces the high electron temperature in Fig. 13(a). These values are in agreement with [20,21], for a direct current plasma jet at atmospheric pressure.

Fig. 14 illustrates the neutral species densities in the plasma, as a function of axial position along the discharge center (a) and radial position, at an axial position of 11 mm from the cathode tip (b). In (a),

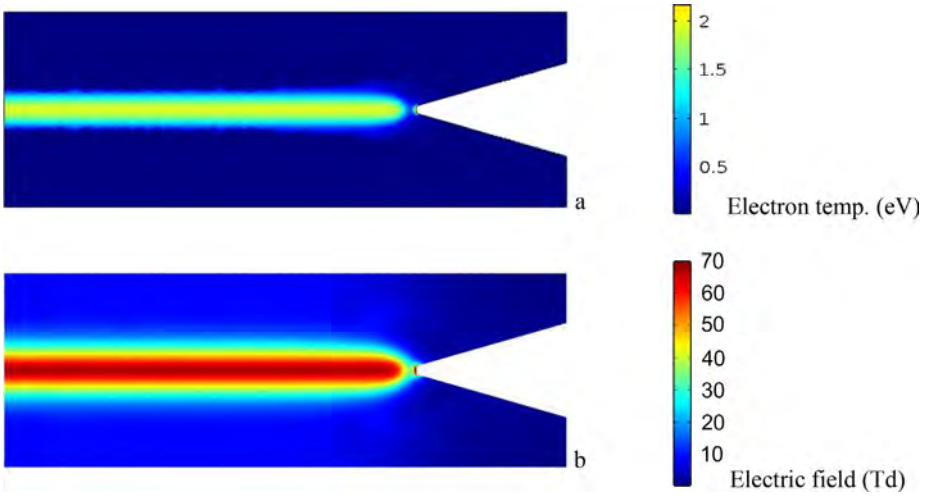

Fig. 13. Calculated electron temperature profile (a) and reduced electric field profile (b), at 25 mA and 3 L/min.

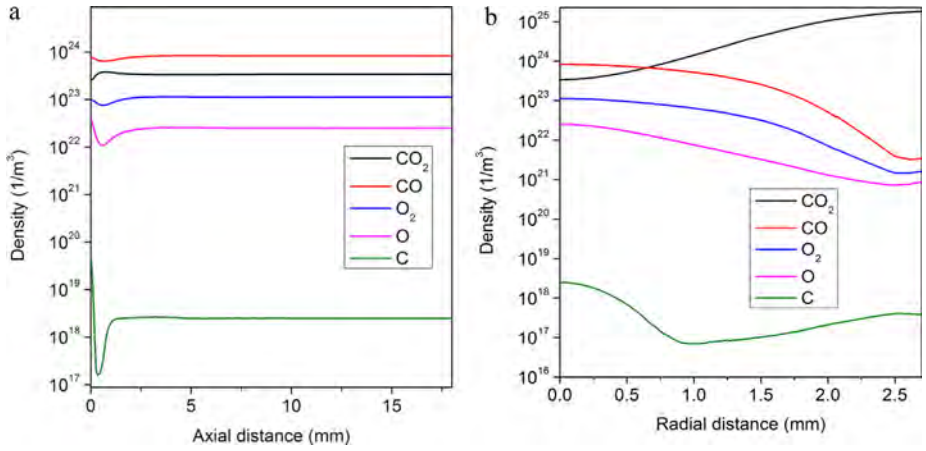

Fig. 14. Axial density distribution, at the discharge center (a), and radial density distribution at an axial position of 11 mm from the cathode tip (b), of the neutral species in the plasma, at 25 mA and 3 L/min.

0 mm corresponds to the cathode tip and 18 mm is the position of the anode. Along the discharge axis, CO is the main plasma species: its density is up to a factor 3 higher than the CO_2 density. This indicates a quite high (~75%) conversion in the center, while it drops rapidly beyond 1 mm from the discharge center (see Fig. 14(b)). The O_2 and O atom densities are also a direct result from the CO_2 dissociation. Upon a splitting reaction, naturally an O atom will be produced, which can further recombine into O_2.

In Table 2, we present the relative contributions of the CO_2 splitting and formation reactions, integrated over the discharge volume. The reason that we present the individual splitting and formation reactions, and not just the net reactions, is that separate CO_2 splitting reactions (i.e., for the CO_2 molecules in vibrational levels and ground state: reactions (1) and (3), and reactions 2 and 5) yield common products, so we cannot simply subtract the formation reactions from the splitting reactions to obtain the net reactions. However, in this way, it looks like 84% of the CO_2 splitting is upon collision with an O atom (with either CO_2 in the vibrational levels or in the ground state), but this accounts only for the forward (splitting) reaction, and not for the reverse reaction, hence it does not represent the net splitting. When looking at the net contribution, this reaction contributes for less than 50%, because the reverse reaction is also very important (90%, cf. Table 2). Indeed, the net contribution of this reaction cannot be more than 50%, because the O atoms must first be created from another CO_2 splitting reaction (e.g., reaction (2), 4 or 5 in Table 2).

The main CO_2 splitting mechanism is the collision of O atoms with vibrationally excited CO_2 molecules, with a relative contribution of 74%. This process is of course initiated by electron impact vibrational excitation of ground-state CO_2 molecules, followed by so-called ladder climbing by vibrational-vibrational relaxation collisions, gradually populating the higher CO_2 vibrational levels, i.e. the so-called "vibrational pathway", as illustrated in Fig. 15.

Table 2
Main CO_2 splitting and formation reactions, and their relative contributions to the total splitting and formation, integrated over the entire plasma volume, at 25 mA and 3 L/min.

	CO_2 splitting	Relative contribution (%)
1.	$O + CO_{2(vib)} \rightarrow CO + O_2$	74.4
2.	$e^- + CO_{2(vib)} \rightarrow e^- + CO + O$	9.79
3.	$O + CO_{2(gr)} \rightarrow CO + O_2$	9.5
4.	$M + CO_{2(vib)} \rightarrow CO + O + M$	3.74
5.	$e^- + CO_{2(gr)} \rightarrow e^- + CO + O$	2.23
	CO_2 formation	Relative contribution (%)
1.	$CO + O_2 \rightarrow CO_2 + O$	90.72
2.	$CO + O + M \rightarrow CO_2 + O$	9.14
3.	$CO + O^- \rightarrow CO_2 + e^-$	0.14

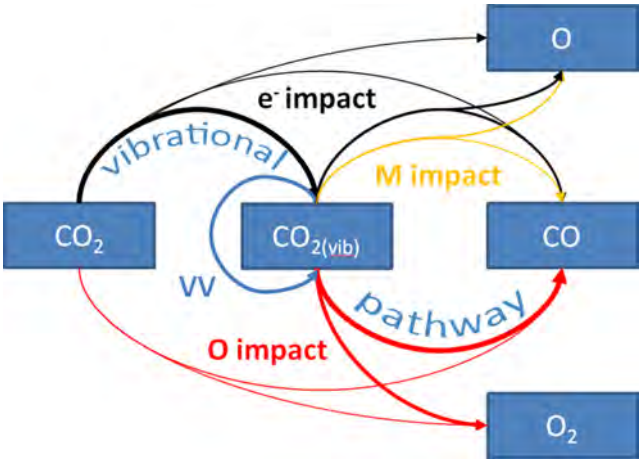

Fig. 15. Reaction scheme of the main CO_2 splitting mechanisms. The main dissociation process is the so-called "vibrational pathway", starting from electron impact vibrational excitation of the CO_2 ground-state molecules, followed by gradually populating the higher vibrational levels through vibrational-vibrational (VV) relaxation collisions, which are then dissociated into CO and O_2 upon impact of O atoms. The dissociation upon O atom impact can also occur from the CO_2 ground-state molecules. In addition, electron impact dissociation, both from CO_2 vibrational levels and ground-state molecules, also contributes to CO_2 splitting, as well as the dissociation upon impact by any molecule in the plasma (M).

The same process also occurs for CO_2 ground-state molecules, with a relative contribution of 9.5%. Besides, electron impact dissociation upon collision with both vibrationally excited and ground-state CO_2 molecules also contributes for about 9.8% and 2.2%, respectively, to the total splitting process. Note that the contribution of electron impact dissociation from the ground state is mainly due to the energetic electrons close to the cathode tip, and because this process is only important in a small region, it explains the low relative importance of this process. Finally, dissociation upon reaction with any other neutral species in the plasma (mainly molecules: M) contributes for 3.7% to the total conversion, again mainly from the CO_2 vibrational levels. Hence, when summing up the splitting reactions upon collision with O atoms or electrons (or other molecules M), with either CO_2 ground-state or vibrational levels, we see that the vibrational levels contribute for about 88% to the CO_2 splitting in the discharge volume, while the ground-state molecules contribute for about 12%. This demonstrates the important role of the CO_2 vibrational levels in the CO_2 splitting process in

the APGD reactor.

When comparing to the mechanisms of CO_2 splitting in a GA plasma, we can see some similarities, but also some differences. Indeed, for a transient AC GA, model calculations predicted a relative contribution of 66% and 19%, for dissociation upon impact of O atoms and electrons with vibrationally excited CO_2, respectively [38]. On the other hand, in the quasi-stationary regime, characteristic for a DC GA, the contributions of these two processes were predicted to be 43% and 40%, respectively, pointing towards very similar contributions for both O atom and electron impact dissociation of the CO_2 vibrational levels [38]. While the APGD can also be interpreted as a quasi-stationary discharge (given that it is also a DC plasma), it is important to note that the model used in [38] was only a 1D model. In [39] a 2D CO_2 model was developed for a classical GA, and the contribution of splitting upon impact of O atoms with vibrationally excited CO_2 molecules was also found to be dominant here (80%), while the same process with ground-state CO_2 contributed for 9.2%, hence very similar to our APGD results. Electron impact dissociation was found to be somewhat less important, while the splitting of CO_2 upon collision with other molecules (M) was higher (7.3% for the vibrational levels). This difference can be attributed to the different type of plasma, different reactor volume and the iterative nature of the classical GA. On the other hand, a 0D modelling study on a GA for CO_2 conversion predicted that electron impact dissociation of vibrationally excited CO_2 was much more pronounced (61–67%), while the splitting upon impact with O atoms contributed only for 7–10% [16]. This can be attributed to the much lower gas temperature assumed as input in this 0D model, i.e., around 1200 K, promoting the electron impact reactions above thermal (neutral) reactions. In [8], a modeling study of a microwave discharge for CO_2 conversion in a wide range of conditions indeed revealed that the dissociation upon impact with O atoms and any molecules (M) becomes more important at higher power deposition (promoting the vibrational excitation) and temperature (promoting neutral (thermal) dissociation reactions above electron reactions). Our simulation results for the gas temperature (Fig. 12(b)) show that the temperature in the APGD is indeed high enough to promote the dissociation reactions upon impact by O atoms.

It is clear that vibrational excitation of CO_2 acts as an effective leverage to the overall CO_2 conversion, and this explains the good energy efficiency obtained in our experiments. However, as can be noted from Fig. 12, the CO_2 conversion only occurs in a small region of the reactor, i.e., along the discharge center, which limits the overall CO_2 conversion, as also seen in our experiments. Indeed, a significant fraction of the gas does not pass through the plasma region, and this was the reason why we developed the confined APGD design, to make sure that all gas will be activated by the plasma, yielding a higher overall conversion.

To elucidate which CO_2 vibrational levels contribute most to the CO_2 splitting, i.e., rather the higher or lower levels, we plot in Fig. 16 the vibrational distribution function (VDF) at the discharge center, at an axial position of 11 mm from the cathode tip, for three different values of electric current. It is clear that the VDF exhibits a Boltzmann distribution, dictated by the gas temperature. Indeed, the dashed line indicates a Boltzmann distribution at a temperature of 2500 K, and it largely coincides with the calculated VDFs. The vibrational temperature is typically obtained from the ratio of the first vibrational level and the ground state:

$$T_{v1} = \frac{E_{v1}}{k\ln(nCO_{2(v1)}/nCO_{2(gr)})} \quad (4)$$

where E_{v1}/k is the energy of the first vibrational state and $nCO_{2(v1)}$, $nCO_{2(gr)}$ stand for the densities of vibrationally excited and ground-state CO_2 molecules, respectively. In Fig. 17, we plot both the vibrational and translational (gas) temperature as a function of radial position, and it is obvious that they are almost identical. They are both around 2500 K along the discharge center (see also Fig. 12(b) above), but they gradually drop to room temperature near the walls. The fact that they are almost equal indicates that the VDF of CO_2 is close to thermal, as is indeed obvious from Fig. 16. This means that the higher vibrational levels are less populated and only the lower vibrational levels of CO_2 actually contribute to the CO_2 conversion. Although the energy efficiency in our experiments is quite good already, it could be further improved if the higher CO_2 vibrational levels could be overpopulated compared to a Boltzmann distribution. This overpopulation is typically realized by vibrational-vibrational (VV) relaxation, as mentioned above, but it is counteracted by vibrational-translational (VT) relaxation, which depopulates the vibrational levels. The latter process becomes more important at high gas temperature. Hence, we believe that a further improvement of the energy efficiency would only be possible if we can let the APGD operate at much lower temperature, i.e., below ca. 1000 K. It was indeed demonstrated by Berthelot and Bogaerts [8] that a non-thermal VDF, with a significant overpopulation of the higher vibrational levels, could only be realized at high power density, while at the same time low gas temperature, but the latter is not easy to realize

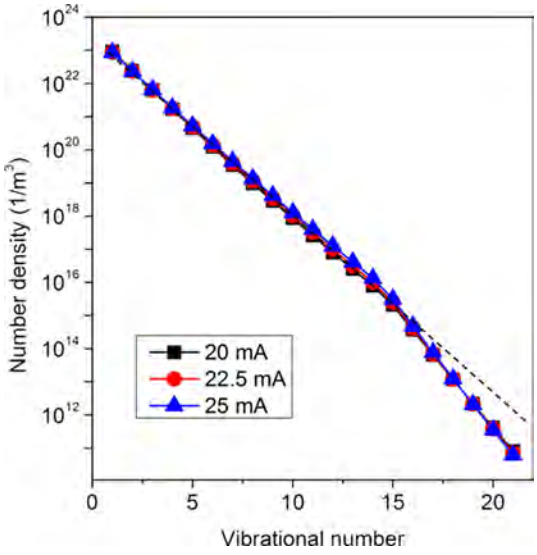

Fig. 16. Vibrational distribution function (VDF) of CO_2, at the discharge center (axial position of 11 mm from the cathode tip), at 3 L/min and three different electrical currents. A Boltzmann distribution at 2500 K is also plotted for comparison (dashed line).

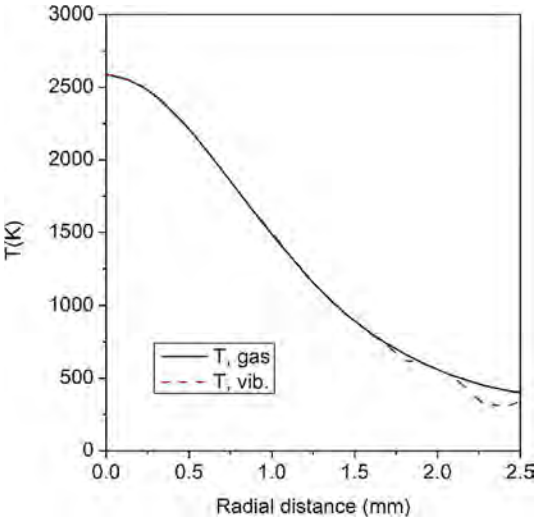

Fig. 17. Radial distribution of the gas and vibrational temperature at an axial position of 11 mm from the cathode tip, at 3 L/min and 25 mA.

at atmospheric pressure [7]. This represents a fundamental challenge for developing atmospheric pressure sources for CO_2 splitting. In future work we will aim to develop a further improved APGD design that can operate at high power density, but at the same time at lower gas temperature.

6. Conclusion

In this work, we thoroughly investigated the potential of a novel plasma reactor for CO_2 conversion, by a combination of experiments and modeling. In the experiments we explored two different reactor improvements with the aid of gas fluid dynamics simulations. In addition, we also developed a fluid plasma model to obtain a better insight in the underlying mechanisms in the plasma, and in the way they affect the performance of the APGD for efficient CO_2 conversion. The basic APGD design shows limited overall CO_2 conversion, which can be explained from the model, because the plasma is only created in a limited region of the reactor, i.e., around the central axis. The calculated conversion inside the plasma region is around 75%, but as a significant fraction of the gas does not pass through this plasma region, the overall conversion is limited to 4.5%. The energy efficiency is fairly good (around 30%), but the model indicates that it could be further improved, because the calculated VDF exhibits a Boltzmann distribution, dictated by the gas temperature. This is due to the significant role of VT relaxation, depopulating the vibrational levels, which is especially important at high gas temperature. Thus, the energy efficiency could be further improved if the higher vibrational levels could be overpopulated, which should be realized by a higher power density, but at the same time reducing the gas temperature.

We therefore proposed some reactor modifications. The vortex-flow AGPD effectively lowers the cathode temperature, and thus allows for operation at higher power, which leads to a higher conversion of about 8%. However, because of the higher power, the gas temperature is still high, limiting the energy efficiency due to a thermal VDF. In addition, still only a limited gas fraction passes through the discharge.

The confined APGD addresses this issue by making use of a ceramic tube with a smaller inner radius of 2.5 mm that fits precisely with the cathode pin. A spiral groove is carved on the pin, guiding the gas into the tube, which acts as effective cooling for the cathode pin, preventing it from melting, and thus also allowing us to use higher power. The plasma region is indeed limited to a radius of 2.5 mm or less, as predicted by the model, so using this ceramic tube with small inner radius makes sure that the plasma fills the entire reactor, and all the gas passes through the active plasma. This gives rise to a higher conversion of 12.5%. However, because the plasma now fills up the entire reactor, it is in contact with the walls, leading to loss of plasma species, as well as heat loss to the walls. For this reason, the energy efficiency is somewhat lower than in the vortex-flow APGD, i.e., around 26%. Nevertheless, the enhancement in conversion is much more significant, i.e., a factor 3 compared to the basic APGD design and a factor 1.5–2 compared to the vortex-flow design. This makes the confined APGD reactor the more cost-effective option for CO_2 conversion.

The plasma model, besides explaining the limited CO_2 conversion in the basic (and vortex-flow) APGD configuration due to the limited fraction of gas passing through the plasma, as well as the limits in energy efficiency due to a thermal VDF, also provides very useful information on other plasma characteristics in the APGD. The calculated electron (or plasma) density of 10^{18} m^{-3} is in reasonable agreement with experimental observations in an APGD (albeit operating at somewhat other conditions and gases, as no experimental data for CO_2 are available in literature). The calculated gas temperature is around 2500 K, which is comparable to measured values in an APGD in air [42], but somewhat lower than in a GAP, where values of 3000 K were calculated for CO_2 [37] and even up to 5500 K were measured for N_2 [17]. This means that the thermal dissociation processes for CO_2 conversion are somewhat lower in the APGD, although still quite significant. Indeed, the vibrational temperature is equal to the gas temperature, and the VDF follows a Boltzmann distribution. The vibrational levels contribute most to the CO_2 splitting, i.e., 88% of the dissociation occurs from the vibrational levels (mainly from the lower levels), while 12% originates from the CO_2 ground state. Indeed, due to the high electric field near the cathode tip, high-energy electrons contribute to the CO_2 splitting with a somewhat larger contribution than in the GAP. However, electron impact dissociation (through electronic excitation) is not the most energy efficient process, so it would be better if we could further exploit the vibrational dissociation pathway by overpopulation of the higher vibrational levels. Nevertheless, the discharge is clearly in non-equilibrium, with the gas temperature being almost 10 times lower than the electron temperature, which was calculated at around 1.9 eV. In addition, the reduced electric field is calculated to be around 60 Td in the discharge center, indicating optimum conditions to maximize the vibrational excitation. Hence, we believe the APGD is a very promising plasma source for CO_2 splitting, especially in the confined configuration, but future efforts should focus on increasing the power density, but at the same time lowering the gas temperature, and thus further promoting the vibrational pathway, to further enhance the CO_2 conversion and energy efficiency. Furthermore, as the gas temperature outside the plasma region is still fairly high, we might expect some contribution from the gas phase chemistry in this region to the CO_2 conversion as well, but this is not yet taken into account in our models. We plan to account for this in our future work, when further finetuning/optimizing the reactor design.

In addition, we plan to further improve our plasma fluid dynamics model, to be able to account for effects that are currently neglected, but which might be important for the reactor design optimization. Indeed, the model would have more predictive power if we could implement a coupled heat transfer and fluid dynamics model, to estimate the cooling power and the inlet gas temperature, as the latter might be important to suppress vibrational-translational relaxations. A fully coupled flow simulation + plasma model is, however, not yet feasible at this stage. Indeed, the Navier-Stokes equations for the flow simulation are solved in 3D, but for the plasma model, we take only the 2D cut-plane of the reactor, because a 3D model including the complete CO_2 chemistry would be prohibitively slow. Therefore, any radial or vortex flow is omitted in the plasma model and the flow vectors are adopted as stationary solution from the 3D model. If we want to make a coupled study, we have to include the flow as time-dependent, and compute it together with the plasma equations, which are also time-dependant. This could slow down the computations by a factor 10, and it is even no guarantee to reach a stable solution. In addition, the solution might not be accurate anymore: the flow would react to the plasma (i.e. due to expansion and buoyance force), but the system would be incomplete without the third vector. Another, simpler approach would be to include a heat zone (instead of plasma) in the flow. However, this raises more questions than answers. Indeed, our aim is to cool down the cathode, but it is not yet clear how much heat is actually produced there. The cathode heats up due to several different and complex mechanisms, including Joule heating, thermionic emission, ion bombardment, and heating from back-scattered electrons. Hence, in order to obtain a proper solution, we would need an accurate cathode spot description, which is a major challenge due to the huge number of reactions and species included in the model. In the confined APGD configuration, the situation would become even more complex, because also the plasma-surface interactions between the plasma and the walls would need to be accounted for. All these effects are outside the scope of our present study, but we plan to study them in our future work. Nevertheless, the present model is already very useful to understand reactor design modifications.

Hence, in spite of the fact that our model could be further improved, we showed in this paper that, using modelling as a main driving force, we could design and test improved APGD configurations, which is more time and cost effective than tedious trial-and-error experiments. In

addition, the support from plasma modeling presents a significant advancement in our understanding of the underlying plasma mechanisms of CO_2 conversion in the APGD.

Acknowledgements

This research was funded by the Fund for Scientific Research Flanders (FWO; Grant numbers 11U5316N and G038316N).

References

[1] Z. Liu, National carbon emissions from the industry process: production of glass, soda ash, ammonia, calcium carbide and alumina, Appl. Energy 166 (2016) 239–244.
[2] J. Qiao, Y. Liu, F. Hong, J. Zhang, A review of catalysts for the electroreduction of carbon dioxide to produce low-carbon fuels, Chem. Soc. Rev. 2 (2014).
[3] T. Schwander, L.S. von Borzyskowski, S. Burgener, N.S. Cortina, T.J. Erb, A synthetic pathway for the fixation of carbon dioxide in vitro, Science 354 (2016) 900–904.
[4] R. Snoeckx, A. Bogaerts, Plasma technology – a novel solution for CO_2 conversion? Chem. Soc. Rev. 46 (2017) 5805–5863.
[5] A. Bogaerts, E. Neyts, Plasma technology: an emerging technology for energy storage, ACS Energy Lett. 3 (2018) 1013–1027.
[6] A. Bogaerts, T. Kozak, K. Van Laer, R. Snoeckx, Plasma-based conversion of CO_2: current status and future challenges, Faraday Discuss. 183 (2015) 217–232.
[7] T. Kozak, A. Bogaerts, Evaluation of the energy efficiency of CO_2 conversion in microwave discharges using a reaction kinetics model, Plasma Sources Sci. Technol. 24 (2015).
[8] A. Berthelot, A. Bogaerts, Modeling of CO_2 splitting in a microwave plasma: how to improve the conversion and energy efficiency, J. Phys. Chem. C 121 (2017) 8236–8251.
[9] A. Fridman, Plasma Chemistry, Cambridge University Press, New York, US, 2008.
[10] W. Bongers, H. Bouwmeester, B. Wolf, F. Peeters, S. Welzel, D. van den Bekerom, N. den Harder, A. Goede, M. Graswinckel, Groen, et al., Plasma-driven dissociation of CO_2 for fuel synthesis, Plasma Process Polym. 14 (2017) e1600126.
[11] R. Aerts, W. Somers, A. Bogaerts, Carbon dioxide splitting in a dielectric barrier discharge plasma: a combined experimental and computational study, ChemSusChem 8 (2015) 702–716.
[12] X. Tu, J.C. Whitehead, Plasma dry reforming of methane in an atmospheric pressure AC gliding arc discharge: co-generation of syngas and carbon nanomaterials, Int. J. Hydrogen Energy 39 (2014) 9658–9669.
[13] J. Liu, H. Park, W. Chung, D. Park, High-efficient conversion of CO_2 in AC-pulsed tornado gliding arc plasma, Plasma Chem. Plasma Process. 36 (2015) 437–449.
[14] M. Ramakers, G. Trenchev, S. Heijkers, W. Wang, A. Bogaerts, Gliding arc plasmatron: providing an alternative method for carbon dioxide conversion, ChemSusChem 10 (2017) 2642–2652.
[15] T. Nunnaly, K. Gutsol, A. Rabinovich, A. Fridman, A. Gutsol, A. Kemoun, Dissoaciation of CO_2 in a low current gliding arc plasmatron, J. Phys. D: Appl. Phys. 44 (2011) 274009.
[16] S. Sun, H. Wang, D. Mei, X. Tu, A. Bogaerts, CO_2 conversion in a gliding arc plasma: performance improvement based on chemical reaction modelling, J. CO_2 Utiliz. 17 (2017) 220–234.
[17] S. Gröger, M. Ramakers, M. Hamme, J. Medrano, N. Bibinov, F. Galucci, A. Bogaerts, P. Awakowicz, Characterization of a nitrogen gliding arc plasmatron using optical emission spectroscopy and high-speed camera, J. Phys. D: Appl. Phys. (2018).
[18] S. Heijkers, A. Bogaerts, CO_2 conversion in a gliding arc plasmatron: elucidating the chemistry through kinetic modeling, J. Phys. Chem. C 121 (2017) 22644–22655.
[19] G. Trenchev, St Kolev, A. Bogaerts, A 3D model of a reverse vortex flow gliding arc reactor, Plasma Sources Sci. Technol. 25–3 (2016).
[20] D. Dudek, N. Bibinov, J. Engelmann, P. Awakowicz, Direct current plasma jet needle source, J. Phys. D: Appl. Phys. 40 (2007) 7367.
[21] N. Bibinov, D. Dudek, P. Awakowicz, J. Engelmann, Characterization of an atmospheric pressure dc plasma jet, J. Phys. D: Appl. Phys. 40 (2007) 7372.
[22] C.L. Wadhwa, High Voltage Engineering, second ed.,, New Age International, 2007, pp. 10–12.
[23] P. Bruggeman, R. Brandenburg, Atmospheric pressure discharge filaments and microplasmas: physics, chemistry and diagnostics, J. Phys. D: Appl. Phys. 46 (2013) 464001.
[24] X.L. Deng, A. Nikiforov, P. Vanraes, Ch. Leys, Direct current plasma jet at atmospheric pressure operating in nitrogen and air, J. Appl. Phys. 113 (2013) 023305.
[25] D. Staack, B. Farouk, A. Gutsol, A. Fridman, Characterization of a dc atmospheric pressure normal glow discharge, Plasma Sources Sci. Technol. 14 (2005) 700–711.
[26] W.S. Boyle, F.E. Haworth, Glow-to-arc transition, Phys. Rev. (1955).
[27] M. Çernákt, E.M. van Veldhuizen, I. Morva, W.R. Rutgers, Effect of cathode surface properties on glow-to-arc transition in a short positive corona gap in ambient air, J. Phys. D: Appl. Phys. 28 (1995) 1126–1132.
[28] D. Shaw, A. West, J. Bredin, E. Wagenaars, Mechanisms behind surface modification of polypropylene film using an atmospheric-pressure plasma jet, Plasma Sources Sci. Technol. 25 (2016) 065018.
[29] V. Brackmann, V. Hoffmann, A. Kauffmann, A. Helth, J. Thomas, H. Wendrock, J. Freudenberger, T. Gemming, J. Eckert, Glow discharge plasma as a surface preparation tool for microstructure investigations, Mater. Charact. 91 (2014) 76–88.
[30] D. Li, X. Li, M. Bai, X. Tao, S. Shang, X. Dai, Y. Yin, CO_2 reforming of CH_4 by atmospheric pressure glow discharge plasma: a high conversion ability, Int. J. Hydrogen Energy 34 (1) (2009) 308–313.
[31] C. Qi, D. Wei, T. Xumei, Y. Hui, D. Xiaoyan, Y. Yongxiang, CO_2 reforming of CH_4 by atmospheric pressure abnormal glow plasma, Plasma Sci. Technol. 8 (2006).
[32] J. Wang, G. Xia, A. Huang, S.L. Suib, Y. Hayashi, H. Matsumoto, CO_2 decomposition using glow discharge plasmas, J. Catal. 185 (1999) 152–159.
[33] A. Bogaerts, C. De Bie, R. Snoeckx, T. Kozák, Plasma based CO_2 and CH_4 conversion: a modeling perspective, Plasma Process. Polym. 14 (2017) e1600070.
[34] W. Wang, R. Snoeckx, X. Zhang, M.S. Cha, A. Bogaerts, Modeling plasma-based CO_2 and CH_4 conversion in mixtures with N_2, O_2, and H_2O: the bigger plasma chemistry picture, J. Phys. Chem. C 122 (2018) 8704–8723.
[35] St Kolev, A. Bogaerts, A 2D model for a gliding arc discharge, Plasma Sources Sci. Technol. (2014) 24-1.
[36] St Kolev, S. Sun, G. Trenchev, W. Wang, H. Wang, A. Bogaerts, Quasi-neutral modeling of gliding arc plasmas, Plasma Processes Polymers 14 (2017).
[37] G. Trenchev, St Kolev, W. Wang, M. Ramakers, A. Bogaerts, CO_2 conversion in a gliding arc plasmatron: multidimensional modeling for improved efficiency, J. Phys. Chem. C 121 (44) (2017) 24470–24479.
[38] W. Wang, A. Berthelot, St Kolev, X. Tu, A. Bogaerts, CO_2 conversion in a gliding arc plasma: 1D cylindrical discharge model, Plasma Sources Sci. Technol. 25 (2016) 065012.
[39] W. Wang, D. Mei, X. Tu, A. Bogaerts, Gliding arc plasma for CO_2 conversion: Better insights by a combined experimental and modelling approach, Chem. Eng. J. 330 (2017) 11–25.
[40] Yu Akishev, M. Grushin, V. Karalnik, A. Petryakov, N. Trushkin, On basic processes sustaining constricted glow discharge in longitudinal N2 flow at atmospheric pressure, J. Phys. D: Appl. Phys. 43 (2010) 215202.
[41] A. Berthelot, A. Bogaerts, Modeling of plasma-based CO_2 conversion: Lumping of the vibrational levels, Plasma Sources Sci. Technol. 25 (2016) 045022.
[42] D. Staack, B. Farouk, A.F. Gutsol, A.A. Fridman, Spectroscopic studies and rotational and vibrational temperature measurements of atmospheric pressure normal glow plasma discharges in air, Plasma Sources Sci. Technol. 15 (2006).
[43] A. Czernichowski, H. Nassar, A. Ranaivosoloarimanana, Spectral and electrical diagnostics of gliding arc, Acta Phys. Pol. A 89 (1996) 595–603.
[44] N. Hasan, D.S. Antao, B. Farouk, DC negative corona discharge in atmospheric pressure helium: transition from the corona to the 'normal' glow regime, Plasma Sources Sci. Technol. 23 (2014) 035013.